NOTES AND CORRESPONDENCE

Reducing Hydrostatic Truncation Error in a Mesobeta Boundary Layer Model

GARY L. ACHTEMEIER

Climate and Meteorology Section, Illinois State Water Survey, Champaign, Illinois

31 January 1990 and 8 August 1990

ABSTRACT

Tiny pressure gradient forces caused by hydrostatic truncation error can overwhelm minuscule pressure gradients that drive shallow nocturnal drainage winds in a mesobeta numerical model. In seeking a method to reduce these errors, a mathematical formulation for pressure gradient force errors was derived for a single coordinate surface bounded by two pressure surfaces. A nonlinear relationship was found between the lapse rate of temperature, the thickness of the bounding pressure layer, the slope of the coordinate surface and the location of the coordinate surface within the pressure layer. The theory shows that pressure gradient force error can be reduced in the numerical model if column pressures are sums of incremental pressures over shallow layers. A series of model simulations verify the theory and show that the theory explains the only source of pressure gradient force error in the model.

1. Introduction

The problem of truncation error within the pressure gradient force terms of numerical models written in sigma coordinates (Phillips 1957) has been the subject of considerable investigation (Kurihara 1968; Gary 1973; Sundqvist 1975, 1976; Janjic 1977; Johnson and Uccellini 1983; Carroll et al. 1987; Janjic 1989). Studies of hydrostatic truncation error as it impacts upon flow near mountains in macroscale numerical prediction models (horizontal grid spacing of the order of 100 km) found the largest truncation errors over sloping terrain where the terrain-following coordinate surfaces depart significantly from pressure surfaces and where the pressure gradient becomes the small difference between two large terms. Some known causes for the truncation errors are small residuals between the two terms of the pressure gradient (Sundqvist 1975; Carroll et al. 1987; Janjic 1977, 1989) and/or vertical interpolation error (Sundqvist 1976; Janjic 1977; Carroll et al. 1987; Johnson and Uccellini 1983).

For high resolution numerical models written in sigma coordinates, hydrostatic truncation error can translate into pressure gradient force errors that overwhelm the minuscule pressure forces that drive weakly forced circulations such as shallow drainage winds within small stream valleys and basins characteristic of the Middle West and South. These drainage flows typically range from 10 cm s^{-1} to 1 m s^{-1}. Therefore, we seek to find how pressure gradient force error enters the model calculations and to find ways to reduce or eliminate the error.

Two tests were conducted using model simulations with initial conditions designed to isolate circulations caused by pressure gradient error. The results of these tests were used to develop a mathematical theory that is applicable for terrain-following coordinate surfaces that slope relative to pressure surfaces. The theory shows how the errors can be reduced so that the numerical calculations are not seriously corrupted. Two additional tests using model simulations verify the theory.

2. Analysis of truncation error

a. Pressure gradient terms

The hybrid numerical prediction model is a shallow-water model with a quasi-Lagrangian integration scheme. The physical dimensions consist of a nocturnal layer that extends from the surface, Z_s, to a height, H, at the top of the nocturnal layer and a free atmospheric layer that extends from H to Z_0, the height of a constant pressure level a few hundred meters above the highest ground. The height of the interface at H is time dependent. The horizontal grid spacing is 20 m. The vertical grid spacing, for this study, is the depth of the nocturnal layer, $H-Z_s$, and the depth of the overlying layer, Z_0-H. The depth of the nocturnal layer is approximately 10 m on hillsides. Over basins, the depth of the nocturnal layer is constrained by the heights of the surrounding hills and can pool up to several 10s of meters.

The nocturnal layer is written in the S-coordinate system:

Corresponding author address: Dr. Gary L. Achtemeier, Southeastern Forest Fire Laboratory, Box 182A, Dry Branch, GA 31020.

$$S = (H - z)/(H - Z_s). \quad (1)$$

The x component of the pressure gradient force term in the S system is

$$\text{PGX} = RT[\delta \ln(p)/\delta x] + g[(1 - S)(\delta H/\delta x) + S(\delta Z_s/\delta x)]. \quad (2)$$

The hydrostatic equation is not transformed.

Consider a layer of atmosphere that is bounded on the top by height Z_1 and on the bottom by height Z_2. The hydrostatic pressure (p_2) at the bottom of the layer at a grid point is given by the pressure (p_1) at the top of the layer and the layer mean temperature as follows:

$$p_2 = p_1 \exp\left[\frac{g}{RT}(Z_1 - Z_2)\right] = p_1 \exp\left[\frac{g}{R} y_{1,2}\right]. \quad (3)$$

Now consider a deep air column that consists of n layers. The pressure, p_n, at height, Z_n, at the base of the column is the pressure, p_0, at the top of the column plus the sum of the incremental pressures contributed by each layer; that is,

$$p_n = p_0 \exp\left[\frac{g}{R} \sum_{k=1}^{n} y_{k-1,k}\right] = p_0 \exp\left[\frac{g}{R} Y_{0,n}\right]. \quad (4)$$

Substitution of (4) into (2) yields the pressure gradient force term for the nocturnal layer,

$$\text{PGX} = g\{T(\delta Y/\delta x) + \delta[(1 - S)H + SZ_s]/\delta x\}. \quad (5)$$

b. Isolating pressure gradient force error

Two tests using model simulations of shallow drainage flows were conducted to isolate hydrostatic truncation error and to develop a method to reduce it. The temperature lapse rates for the nocturnal boundary layer and the free atmosphere layer above it were dry adiabatic. This static atmosphere allows no horizontal pressure gradients other than pressure variations that resulted from changes in elevation. Any circulations generated by the model were, therefore, a measure of the pressure gradient force error. Flow-through boundary conditions required no special boundary formulations except where the flow was directed into the domain. Then extrapolated boundary conditions were used; that is, the adjacent velocity at the previous time level was assigned to the boundary. The results of these tests are described below.

1) TEST 1

A surface (Fig. 1) that is level at 30-m elevation to the left of the figure slopes down to 0 m over a distance of 300 m. The maximum slope along the hillside is 0.15. A small valley separates the hillside from a small ridge 12 m high located near the center of the domain. Elevations descend gradually from the ridge into a broad basin. The land form is oriented along the x-axis. It extends infinitely in y and, therefore, all derivatives with respect to y are zero. The 50 grid points are spaced at 20-m intervals so that the land form spans a distance of 1 km. A 10-m deep nocturnal boundary layer (dashed line in Fig. 1) paralleled the surface.

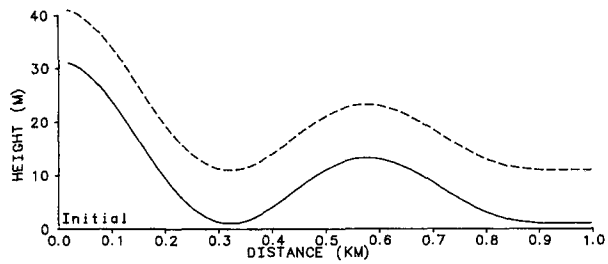

FIG. 1. Initial conditions for test 1 showing shape of land form and overlying nocturnal layer (dashed line).

Results after 21 min of integration are shown in Fig. 2a. The pressure gradient error systematically forced downslope flow. Error velocities of approximately 10 cm s^{-1} were found along the steeply sloping hillside. Mass convergence into the valley doubled the depth of the nocturnal layer (upper solid line).

The maximum error velocity after 60 min was 19 cm s^{-1} (Fig. 2b). Mass convergence into the valley tripled the depth of the nocturnal layer. In addition, the error velocity reversed direction and was flowing upslope along the side of the ridge at distances between 0.4 and 0.5 km.

The behavior of the error velocities near the ridge needs further explanation. The mean pressure gradient for the nocturnal layer was used to calculate the error velocity. Therefore, the results in Fig. 2 are for the layer, mean error velocity. During the course of the simulation, mass mounded up the nocturnal layer in the valley to the extent that after 60 min of integration the slope of the coordinate surface at the top of the nocturnal layer had reversed and become steeper than the slope of the ridge. Therefore, the mean slope of the coordinate surfaces for the layer changed the sign of the mean error pressure gradient. The latter reversed the error velocity along the left side of the ridge.

2) TEST 2

The finding from test 1 that the error velocity depends upon the mean slope of the coordinate surfaces, not just the slope of the terrain, was used to design a second test to determine if error velocities are excited if the surface is flat but the coordinate surface within the domain slopes as in Fig. 1. All of the initial conditions were identical to those of test 1 with the exception of the flat surface. The top of the nocturnal layer at H (Fig. 3) slopes as in test 1. Figure 4a shows that pressure gradient errors after 11 min of integration have

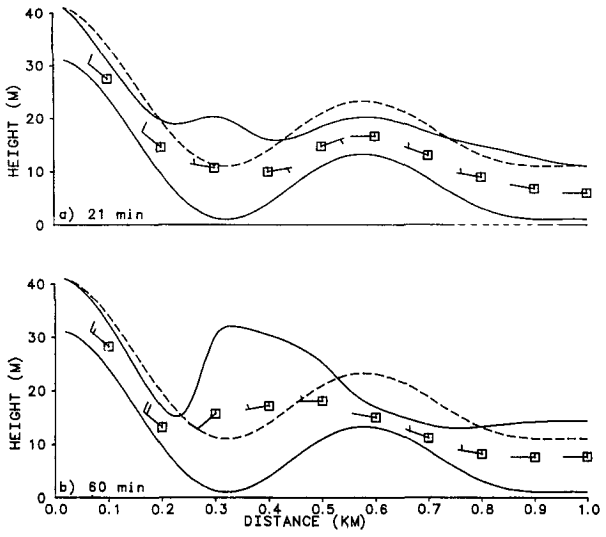

FIG. 2. Test 1 error velocities (short barb = 5 cm s^{-1}; long barb = 10 cm s^{-1}) and growth of error height of the nocturnal layer after (a) 21 min and (b) 60 min of model integration.

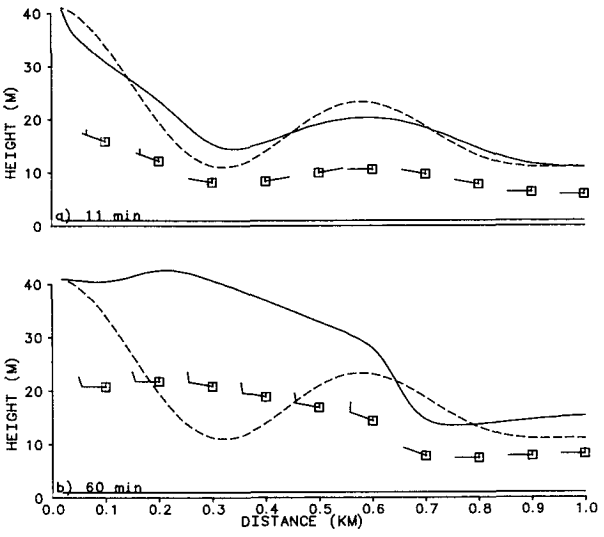

FIG. 4. Test 2 error velocities and growth of error height of the nocturnal layer after (a) 11 min and (b) 60 min of model integration.

forced error velocities down the slope of the coordinate surface at H. By 60 min of integration (Fig. 4b), the error velocities blow continuously from left to right.

Both tests have shown that the directions and magnitudes of the error velocities depend upon the slopes of the coordinate surfaces. In the second test, the only differences between pressures calculated at adjacent grid points were the elevations of the interface, H. Though the total depth over which the pressure was calculated was 500 m for all grid points, the depths of the nocturnal layer and of the free atmosphere that make up the column were not the same. Therefore, one should expect the hydrostatic pressures calculated over unequal finite intervals to be slightly different at adjacent grid points. Thus, hydrostatic truncation error is not a problem of truncation but a result of approximating an integral by vertically averaging the temperature over finite layers. The inexactitude that results from approximating the hydrostatic equation has been extensively documented in the literature already cited.

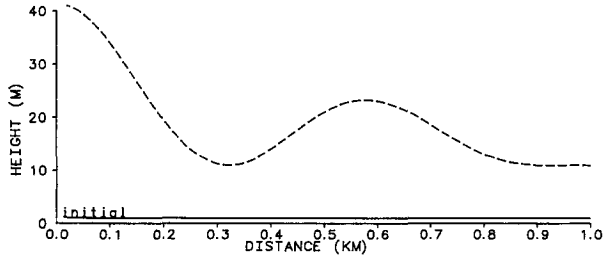

FIG. 3. Initial conditions for test 2 showing flat land form and overlying nocturnal layer (dashed line).

c. *A theory for pressure gradient force error*

The pressure gradient force error is now defined from a mathematical perspective. The derivation is modeled after the initial conditions for test 2 (Fig. 3). The top of the domain is defined as a pressure surface. The lower coordinate surface is flat and also a pressure surface. The mathematical expression is derived for pressure gradient force error at the lower coordinate surface. At the surface, $S = 1$ and $Z_s = 0$, and the height correction term of (5) vanishes. The pressure gradient force term is thus,

$$\mathrm{PGX} = gT(\delta Y/\delta x). \tag{6}$$

Consider in Fig. 5 a vertical cross section of atmosphere bounded on the sides by two grid columns and

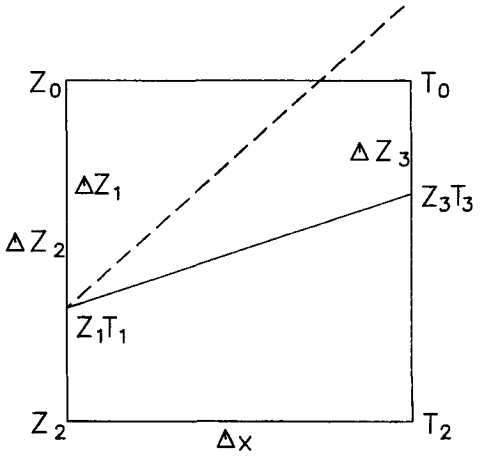

FIG. 5. Simple grid column bounded on top and bottom by constant pressure surfaces. Sloping coordinate surfaces (solid and dashed lines) pass through the grid column as shown.

on the top (Z_0) and bottom (Z_2) by constant pressure surfaces. The isotherms are horizontal and the temperature lapse rate is a constant Γ. If the hydrostatic pressure is approximated over the depth, $Z_2 - Z_0$, then there exists a small residual given by

$$E_H = P_0\left[\exp\left(\int_0^2 \frac{g}{RT}\,dZ\right) - \exp(gY_{20}/R)\right]. \quad (7)$$

However, the residual at the neighboring grid point is the same. Therefore, the horizontal derivative of E_H vanishes in the calculation of the pressure gradient error.

Pressure gradient force errors appear when the calculation of Y_{20} is done differently at neighboring grid points. Let an S-coordinate surface intersect the layer in Fig. 5, passing through it at depth Z_1 at the first grid column and at depth Z_3 at the second grid column; both depths being measured downward from the top. For the left grid column (4) yields

$$Y_{20} = y_{21} + y_{10} = \frac{Z_2 - Z_1}{T_{21}} + \frac{Z_1 - Z_0}{T_{10}}, \quad (8)$$

and for the right grid column,

$$Y'_{20} = y_{23} + y_{30} = \frac{Z_2 - Z_3}{T_{23}} + \frac{Z_3 - Z_0}{T_{30}}. \quad (9)$$

From (6) the pressure gradient force error is

$$\text{PGE} = gT_2\epsilon/\Delta x \quad (10)$$

where $\epsilon = Y'_{20} - Y_{20}$. Clearly, ϵ is proportional to the pressure gradient force error with the proportionality constant for the conditions specified by (10) being $gT_2/\Delta x$. Therefore, the behavior of ϵ determines the behavior of the pressure gradient force error. From the definitions (8) and (9),

$$\epsilon = 2\left[\frac{Z_2 - Z_3}{T_2 + T_3} + \frac{Z_3 - Z_0}{T_3 + T_0} - \frac{Z_2 - Z_1}{T_2 + T_1} - \frac{Z_1 - Z_0}{T_1 + T_0}\right]. \quad (11)$$

Let $Z_0 - Z_i = \Delta Z_i$. Furthermore, let $T_i = T_0 + \Gamma\Delta Z_i$ where Γ is the lapse rate of temperature over the interval. Since $\Delta T_i = \Gamma\Delta Z_i$ is only a few percent of the total temperature, it may be neglected from the denominator of the error equation. After some algebraic expansion, (11) becomes the cubic polynomial,

$$\epsilon = (aT_0^3 + bT_0^2\Gamma + cT_0\Gamma^2 + d\Gamma^3)/(2T_0^4) \quad (12)$$

where

$$a = 0,$$
$$b = 0,$$
$$c = 4\Delta Z_2[\Delta Z_1(\Delta Z_1 - \Delta Z_2) + \Delta Z_3(\Delta Z_2 - \Delta Z_3)],$$
$$d = 4\Delta Z_1\Delta Z_2\Delta Z_3(\Delta Z_1 - \Delta Z_3).$$

Define α and α' to represent the fraction of the total depth of the layer ΔZ_2 and the S-coordinate surface is found from the top of the layer. Therefore, let $\alpha = \Delta Z_1/\Delta Z_2$ and $\alpha' = \Delta Z_3/\Delta Z_2$. Equation (12) simplifies to

$$\epsilon = 2\Gamma^2\left(\frac{\Delta Z_2}{2T_0}\right)^3\left\{-w(\alpha, \alpha') + \frac{\Gamma\Delta Z_2}{T_0}[\alpha\alpha'(\alpha - \alpha')]\right\} \quad (13)$$

where

$$w(\alpha, \alpha') = \alpha(1 - \alpha) - \alpha'(1 - \alpha').$$

Both terms involving α and α' are of the same order of magnitude. Therefore, for temperature lapse rates less than the dry adiabatic lapse rate and for layer thicknesses less than 1 km, the second term of (13) is at least two orders of magnitude smaller than the first. Upon neglecting the second term, the equation for the pressure gradient force error is

$$\text{PGE} = \frac{gT_2}{\Delta x}\left[-2\Gamma^2\left(\frac{\Delta Z_2}{2T_0}\right)^3 w(\alpha, \alpha')\right]. \quad (14)$$

The pressure gradient force error vanishes as the lapse rate of temperature approaches the isothermal lapse rate. PGE is largest when Γ is dry adiabatic or if there exists a large temperature inversion. The relationship between PGE and the square of Γ confirms the results of Carroll et al. (1987) who observed that spurious horizontal accelerations increased by 100 for each increase by 10 of the lapse rate.

The nonlinear function $w(\alpha, \alpha')$ carries information on the slope of the coordinate surface and the height at which the coordinate surface intersects the column. The relationships between α, α', and $w(\alpha, \alpha')$ and therefore PGE are shown in Fig. 6. The quantity $w(\alpha, \alpha')$ has been normalized by its maximum numerical

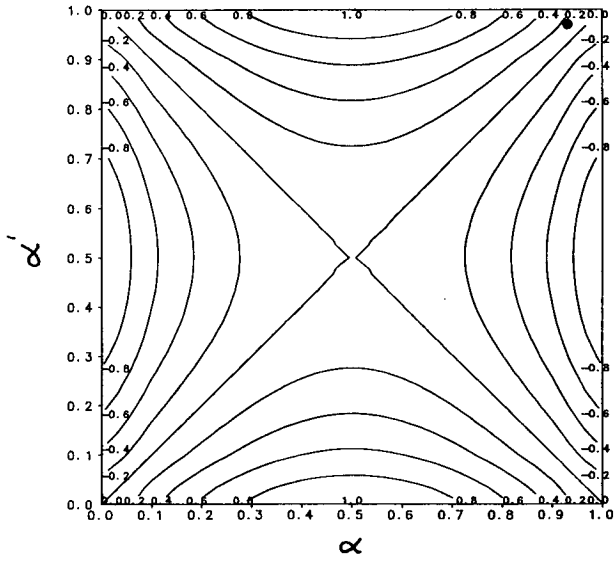

FIG. 6. The distribution of normalized $w(\alpha, \alpha')$ with respect to α and α'.

value of 0.25. Given that α and α' are fractions of the depth of the pressure layer as measured downward from the top, Fig. 6 can be interpreted as follows:

1) When ($\alpha = \alpha'$), the S-coordinate surface is horizontal and thus becomes a constant pressure surface. The pressure gradient force error is zero for this trivial case. Therefore, $w(\alpha, \alpha') = 0$ along the ascending diagonal.

2) If the S-coordinate surface is located such that $\alpha = 1 - \alpha'$, the pressure gradient force error vanishes and $w(\alpha, \alpha) = 0$ along the descending diagonal in Fig. 6. The requirement is that the coordinate surface is located the same distance from the top of a grid column as it is from the bottom of an adjacent grid column, both column depths being equal.

3) The sign of PGE is determined by both the slope of the coordinate surface and its position within the column. Consider for example the S-coordinate surface located at the first grid column so that $\alpha = 0.3$. Then, $\alpha' = 0.5$ yields $w(\alpha, \alpha') < 0$, but if $\alpha' = 0.8$, $w(\alpha, \alpha') > 0$.

The complex interplay between the location and slope of the coordinate surface makes the interpretation of $w(\alpha, \alpha')$ somewhat ambiguous. Further insight may be gained through expressing α' as a function of α and the slope β of the coordinate surface. Reference Fig. 5 for a schematic of the relationship of the variables that take part in the transformation. From the definitions, $\alpha = \Delta Z_1/\Delta Z_2$ and $\alpha' = \Delta Z_3/\Delta Z_2$, we find

$$\alpha' = \alpha - \Delta x \tan(\beta)/\Delta Z_2. \quad (15)$$

The quantity $\Delta x/\Delta Z_2 = 1$ is chosen to isolate slope information in β. Substitution of these definitions into $w(\alpha, \alpha')$ yields,

$$w(\alpha, \beta) = \tan(\beta)[1 - 2\alpha + \tan(\beta)]. \quad (16)$$

Figure 7 shows that the distribution of $w(\alpha, \beta)$ can be of either sign depending upon where the coordinate surface enters the grid column (α carries this information). Therefore, pressure gradient force error may act to drive error velocities downslope at some points in a model and drive error velocities upslope at other points. The curves for α in the 0.7–0.8 range are similar to the distribution of normalized spurious horizontal acceleration found by Carroll et al. (1987) for the same range of slope angles. The interpretation of the shape of these curves differs from that of Carroll et al., however, because in the present case, the pressure gradient force error is calculated for the surface. The surface is horizontal, coincident with a surface of constant pressure, and the pressure gradient is given by a single term.

Only the α term [second term in brackets in (16)] is negative and, therefore, only the location where the coordinate surface enters the grid column can force $w(\alpha, \beta) < 0$. Figure 8 gives a graphical perspective of seven entry points for a surface that slopes at 20° within

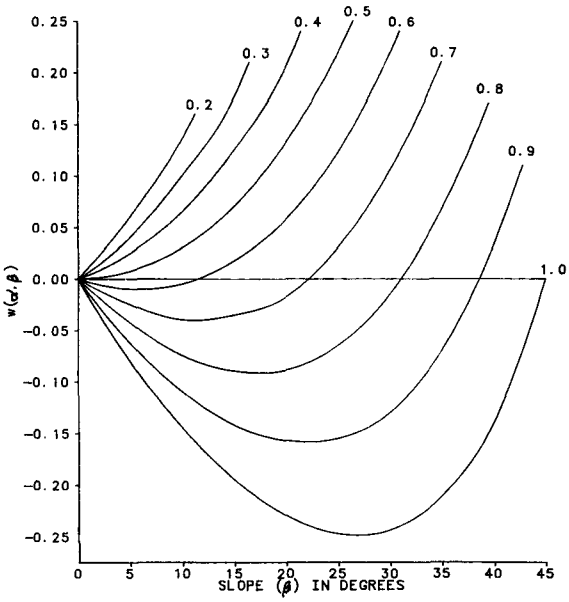

FIG. 7. Relationship between $w(\alpha, \beta)$ and slope angle of a coordinate surface for selected entry points into the grid column. Entry points given in terms of the ratio α.

a regular grid column. Figure 9 shows that $w(\alpha, \beta)$ for these seven placements decreases linearly as the entry point is moved down the grid column from $\alpha = 0.4$–1.0. The quantity $w(\alpha, \beta)$ changes sign if the coordinate surface enters the grid column about two-thirds down from the top (approximately $\alpha = 0.7$). The sign change occurs at precisely where $\alpha = 1 - \alpha'$ in Fig. 6.

One can use (14) to calculate the maximum error velocity under the conditions of test 1, and compare the results with error velocities obtained from the numerical model after 21 min of integration. The calculation was done for a slope equal to the average slope of a 120-m section of the steepest part of the hillside shown in Fig. 1. This interval was chosen because a particle moving at 10 cm s^{-1} for 20 min will transverse 120 m. The maximum error velocity was observed at the hillside location (see Fig. 2). In addition, the relative locations of the top of the nocturnal layer and the top of the grid column were the same as in the numerical model. The $w(\alpha, \alpha')$ for the hillside location is given by the solid circle near the upper right corner of Fig. 6. Substitution of the appropriate variables into (14) and multiplying the resulting pressure gradient force error by 21 min gave a predicted maximum error velocity along the hillside of 10.5 cm s^{-1}. The maximum error velocity found in the test 1 simulation was 9.5 cm s^{-1}. Therefore, allowing for the obvious differences between methods for obtaining error velocities, it is found that (14) explains all of the maximum error velocity observed from the numerical model. The model sensitivity tests that follow further confirm this finding.

d. Reducing pressure gradient error

Various methods to reduce the PGE have been presented in the literature. Most of the methods involve the development of specialized finite difference schemes that reduce or eliminate PGE. Another approach has been to define an exact form for the temperature to eliminate the hydrostatic truncation error. In the above approaches, however, the functional form for the PGE may not be that given in (14).

As regards the mesobeta numerical model, the pressure gradient force error can be reduced in two ways. First, in calculating the hydrostatic pressure, choose the height interval containing the S-coordinate surface so that the condition $\alpha = 1 - \alpha'$ is satisfied exactly. Then $w(\alpha, \alpha') = 0$ and the PGE vanishes.

The second approach to reducing the PGE is to make ΔZ_2 as small as possible. Equation (14) shows that the PGE is reduced a 1000-fold for every 10-fold decrease in the vertical separation. Two new tests were designed to further show that (14) explains the error velocities observed in the numerical model.

1) TEST 3

Five model runs were made using the same initial conditions as for Test 1. For each run, the hydrostatic pressure for the atmospheric column from 500 m to the ground was calculated by dividing the columns into successively thinner layers and obtaining the final pressure as the sum of incremental pressures. The layer thicknesses were 250, 100, 50, 20 and 10 m. Then the maximum error velocities obtained from the model simulations were compared with maximum error velocities predicted by (14). As the layer thicknesses are made smaller, there are increasing possibilities that the coordinate surface and the pressure surfaces will cross somewhere between grid points at one or more points within the domain. No effort was made to test for this. If pressure surface–coordinate surface intersections increase the PGE, the errors should be observable in the simulations.

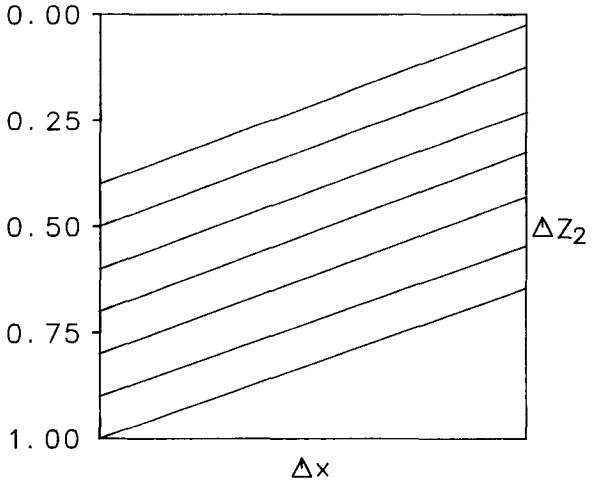

FIG. 8. Seven placements of a 20° slope coordinate surface within a grid column bounded by pressure surfaces.

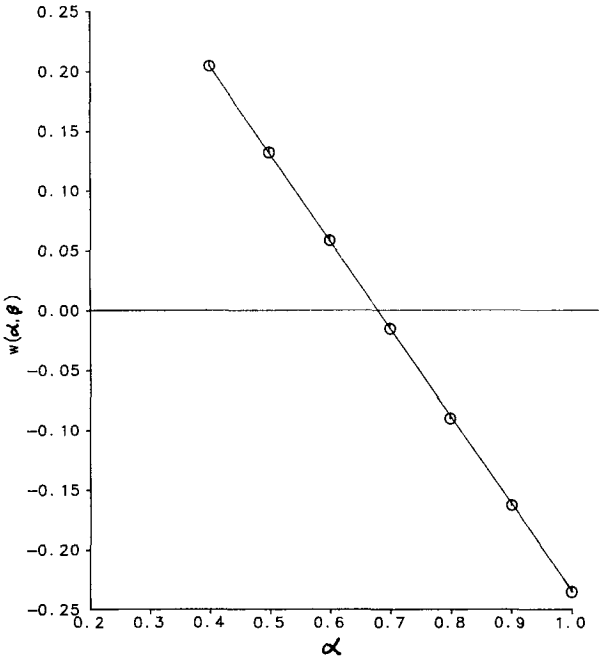

FIG. 9. Relationship between $w(\alpha, \beta)$ and α for a coordinate surface sloping at 20°.

The results of the five runs are summarized in Table 1 for error growth after 60 min of integration. The maximum error velocity and the growth of the maximum error height of the nocturnal layer expressed as a percentage of the initial height are given for the five layer thicknesses. The velocity errors for test 1 (*UL*) are included for reference. Each reduction in the layer thickness was accompanied by a significant reduction in the error velocities and heights. When the 10 m thickness was used, the maximum error velocity was only 30 μm s^{-1} and the maximum error in the height of the nocturnal layer was only 1.7 cm. The fourth column of Table 1 gives the maximum error velocities predicted by (14). Given the differences in the methods for calculating the error velocities, these compare favorably in magnitude with the maximum error velocities found from the numerical simulations.

2) TEST 4

Are there any other sources of pressure gradient error within the model not explained by (14)? The initial conditions for the model run were identical as those for test 1 with the exception that the lapse rate of temperature was isothermal instead of dry adiabatic. Since ϵ is zero for an isothermal atmosphere, any growth of error velocities during test 4 must arise from a source

TABLE 1. Maximum error velocities and percent growth of maximum error heights after 60 min of integration of numerical model for selected layer thicknesses and maximum error velocities predicted from theory.

Max layer thickness (m)	Max error velocity (cm s^{-1})	Percent growth max error height	Predicted max error velocity (cm s^{-1})
UL	19.4	208.0	—
250	5.2	125.0	8.3
100	0.72	19.2	1.2
50	0.11	3.3	0.23
20	0.024	0.81	0.007
10	0.003	0.17	0.002

other than horizontal variations of hydrostatic truncation error. The model ran for 60 min and generated no error velocity.

3. Discussion

When the pressure–height relationship is calculated through an approximation to the integral hydrostatic equation, there will remain a small residual "hydrostatic truncation" error. If the coordinate surfaces slope relative to constant pressure surfaces, the hydrostatic truncation errors will be slightly different at adjacent grid points. The resulting tiny pressure gradient force errors are sufficient to generate error velocities large enough to overwhelm meteorological velocities produced in a mesobeta-scale wind model written in terrain-following coordinates.

A mathematical analysis found that pressure gradient force error depends upon the lapse rate of temperature, the thickness of the pressure layer through which passes a sloping coordinate surface, the slope of the coordinate surface, and the location of the coordinate surface within the layer. PGE can be of either sign depending upon the location of the coordinate surface within the layer.

The equation showed two ways in which the PGE could be reduced or eliminated. Error velocities were reduced by calculating hydrostatic pressures as the sum of incremental pressures over shallow layers. It would seem that the only limitation on completely eliminating PGE is the number of calculations required to obtain the total column pressure. However, Mahrer (1984) found errors in horizontal gradients of meteorological fields when the distance between two vertical grid points is smaller than the distance between two horizontally adjacent terrain-following coordinate points. Although the geometry of the development presented here differs from the problem design of Mahrer, it is recognized that allowing coordinate surfaces to cross pressure surfaces between grid points may increase the PGE.

The curves of $w(\alpha, \alpha')$ in Fig. 7 all terminate at the upper right of the grid column in Fig. 5. The positive curvatures are an indication that much larger $w(\alpha, \alpha')$ should be expected if the coordinate surface crossed the pressure surface between grid points. In that event, the coordinate surface intersects the grid column above Z_0 as is shown by the dashed line in Fig. 5. The interval ΔZ_3 is directed upward (the convention of integration is downward) and ΔZ_3 is negative. Therefore, $w(\alpha, \alpha') = \alpha(1 - \alpha) + \alpha'(1 + \alpha')$. For steeper coordinate surfaces slopes, the first term becomes negligible and $w(\alpha, \alpha') = w(\alpha') \approx (\alpha')^2$. Thus, when coordinate surfaces cross pressure surfaces between grid points, growth of $w(\alpha')$ can offset small ΔZ_2 and cause growth in the PGE.

Mahrer suggested that the horizontal grid spacing be reduced so that the sloping coordinate surfaces would be contained within a single pressure interval. The horizontal grid spacing of 20 m used throughout this study was sufficient to satisfy Mahrer's criteria.

Acknowledgments. This research was funded by the U.S. Southeastern Forest Experiment Station under Grant USDA 29-412.

REFERENCES

Carroll, J. J., L. R-Mendez-Nunez and S. Tanrikulu, 1987: Accurate pressure gradient calculations in hydrostatic atmospheric models. *Bound. Layer Meteor.*, **41,** 149–169.

Gary, J. M., 1973: Estimate of truncation error in transformed coordinate primitive equation atmospheric models. *J. Atmos. Sci.*, **30,** 223–233.

Janjic, Z. I., 1977: Pressure gradient force and advection scheme used for forecasting with steep and small-scale terrain. *Beitr. Phys. Atmos.*, **50,** 186–199.

——, 1989: On the pressure gradient force error in σ-coordinate spectral models. *Mon. Wea. Rev.*, **117,** 2285–2292.

Johnson, D. R., and L. W. Uccellini, 1983: A comparison of methods for computing the sigma-coordinate pressure gradient force for flow over sloped terrain in a hybrid theta-sigma model. *Mon. Wea. Rev.*, **111,** 870–886.

Kurihara, Y., 1968: Note on finite difference expressions for the hydrostatic relation and pressure gradient force. *Mon. Wea. Rev.*, **96,** 654–656.

Mahrer, Y., 1984: An improved numerical approximation of the horizontal gradients in a terrain-following coordinate system. *Mon. Wea. Rev.*, **112,** 918–922.

Phillips, N. A., 1957: A coordinate system having some special advantages for numerical forecasting. *J. Metor.*, **14,** 184–185.

Sundquist, H., 1975: On truncation errors in sigma-system models. *Atmosphere*, **13,** 81–95.

——, 1976: On vertical interpolation and truncation in conexion with use of sigma system models. *Atmosphere*, **14,** 37–52.